The Canadian Mineralogist
Vol. 37, pp. 575-591 (1999)

THE GUIBARÉ AND FÉTÉ KOLÉ GOLD-BEARING TOURMALINE–QUARTZ VEINS IN THE BIRIMIAN GREENSTONE BELTS OF BURKINA FASO

DIDIER BÉZIAT[1], FRANÇOIS BOURGES AND PIERRE DEBAT

Laboratoire de Minéralogie et Cristallographie, UMR 5563, Université Paul Sabatier, 39, allées Jules Guesde, F-31000 Toulouse Cedex, France

YVES FUCHS

Laboratoire de Minéralogie et Cristallographie, URA 09, Université Pierre et Marie Curie, 4, place Jussieu, F-75252 Paris Cedex 05, France

MARTIN LOMPO

Département de Géologie, FAST, Université de Ouagadougou, Ouagadougou, Burkina Faso

FRANÇOIS MARTIN

Laboratoire de Minéralogie et Cristallographie, UMR 5563, Université Paul Sabatier, 39, allées Jules Guesde, F-31000 Toulouse Cedex, France

SERGE NIKIÉMA

B.H.P. Ouagadougou, Burkina Faso

FRANCIS TOLLON

Laboratoire de Minéralogie et Cristallographie, UMR 5563, Université Paul Sabatier, 39, allées Jules Guesde, F-31000 Toulouse Cedex, France

Abstract

The Guibaré and Fété Kolé deposits in Burkina Faso consist of Birimian gold-bearing quartz and tourmaline veins in metamorphosed volcano-sedimentary formations of an Early Proterozoic greenstone belt. Tourmaline compositions for the two prospects vary according to occurrence: dravite in the Guibaré deposit, hosted by metabasic to meta-ultrabasic rocks, in contrast to schorl in the Fété Kolé deposit, hosted by metasedimentary and metavolcanic rocks. The major control on tourmaline composition thus seems to be the Mg/(Mg + Fe) value of the host rock rather than the composition of the hydrothermal fluid. In both deposits, the gold is not associated with sulfides, but rather is concentrated within tourmaline layers, typically at the tips of the tourmaline crystals and as small grains filling fractures in tourmaline. Mössbauer and infrared spectroscopic data show the presence of ferric iron coupled with evidence of deprotonation in these tourmalines, indicating a relatively oxidizing environment for the Au deposits. A drop of fluid pressure and deprotonation could have induced physicochemical changes that caused deposition of the gold.

Keywords: tourmaline, gold, electron-microprobe data, Mössbauer data, infrared data, Birimian, Burkina Faso.

Sommaire

Les filons de quartz aurifères à tourmaline des gîtes de Guibaré et Fété Kolé apparaissent au sein des formations métavolcanosédimentaires des ceintures de roches vertes du Burkina Faso. La composition chimique des tourmalines varie avec la nature des roches encaissantes: dravite au sein des roches basiques à ultrabasiques de Guibaré, schorl dans les niveaux métavolcaniques de Fété Kolé, ce qui est conforme à une hypothèse d'un faible rapport eau/roche dans le système hydrothermal.

[1] *E-mail address*: dbeziat@cict.fr

Dans ces deux gîtes, l'or n'est pas associé aux sulfures mais directement à la tourmaline, soit à la surface des cristaux, soit en remplissage des microfissures. Les données infrarouge et Mössbauer mettent en évidence une déshydroxylation et la présence de fer trivalent dans ces tourmalines, indiquant des conditions relativement oxydantes au moment du dépôt de l'or. La diminution de la pression dans la phase fluide et la déprotonation de la tourmaline seraient les facteurs responsables de la précipitation de l'or dans ces gisements.

Mots-clés: tourmaline, or, données de microsonde électronique, données en spectroscopie infrarouge, données en spectroscopie de Mössbauer, birimien, Burkina Faso.

Introduction

Gold deposits in which the gold is paragenetically closely related to tourmaline are somewhat rare (*e.g.*, Slack 1996); among the few well-documented examples are the gold deposits of the Sigma mine, in the Abitibi greenstone belt of Quebec (Robert & Brown 1986, Robert & Kelly 1987), and of the Hemlo area of Ontario (Gustafson 1995). In the Early Proterozoic Birimian (~2 Ga) greenstone belts of West Africa, two types of tourmaline-bearing gold deposits have been described (Milési *et al.* 1989, 1992): i) those hosted by turbidites (sandstone and rare conglomerate), which were affected by the two main Eburnean tectonometamorphic phases (Loulo district, western Mali), and ii) mesothermal Au and tourmaline–quartz veins with rare polymetallic sulfides that correspond to gold-bearing shear zones. However, in both types of deposit, gold formed in association with the sulfide mineralization but not the tourmaline (Huot *et al.* 1987, Milési *et al.* 1992). In this paper, we describe two new occurrences of tourmaline and gold deposits from the Birimian greenstone belts of Burkina Faso: Guibaré, 75 km north of Ouagadougou, and Fété Kolé, near the Mali border (Fig. 1). Features of these

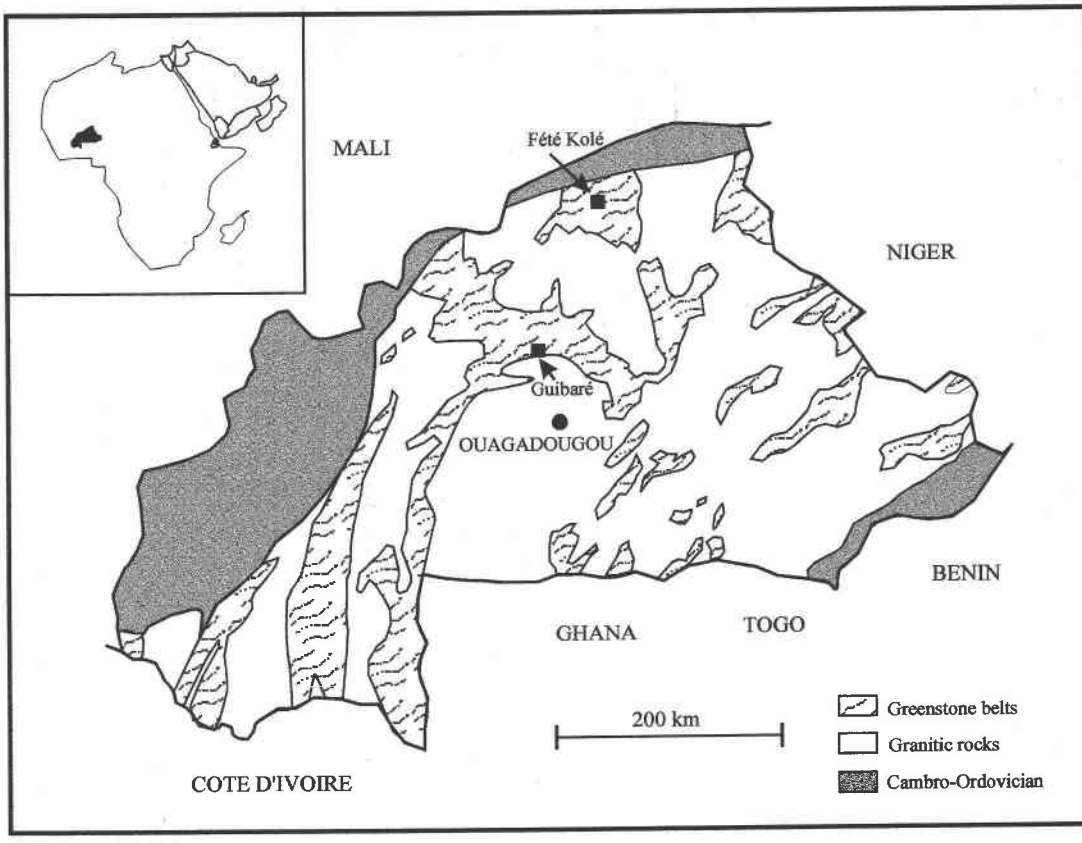

FIG. 1. Geological sketch-map of Burkina Faso showing the location of the occurrences studied.

occurrences are used to consider processes responsible for the gold mineralization.

Geology

Gold-bearing tourmaline–quartz veins at Guibaré and Fété Kolé are found within a large high-strain zone (regional shear-zone, 150 to 300 m wide and 2 to 5 km long) characterized by the development of a pervasive vertical foliation and intense hydrothermal alteration (Figs. 2A, B). The gold mineralization is found in quartz–tourmaline veins of various width (1 cm to 2 m) and length (some dm to 50 m, Fig. 3); these veins are generally shallowly dipping and strongly folded, with common development of ptygmatic structures. Within the veins, clusters of small tourmaline crystals are folded, whereas recrystallized microsaccharoidal quartz grains are elongate parallel to the foliation (and the axial plane, Fig. 4A). In both deposits, crystallization of the tourmaline predates the folding and foliation.

In the Guibaré prospect, the host rocks are ultrabasic to basic. These rocks contain chlorite, ferroan dolomite, quartz, and relict chromite, and have high contents of Mg (12 wt % MgO), Cr (1700 ppm), and Ni (330 ppm) and a high Mg# [$Mg/(Mg + Fe^{2+}) = 0.75$]. In the Fété Kolé prospect, the host rocks are: i) metasedimentary rocks (metapelites), essentially containing white mica (phengite) with minor amounts of quartz, and ii) metavolcanic rocks, with chlorite, ilmenite, quartz, clinozoisite and calcite, with a lower Mg# (0.35), MgO (3 wt %), Cr (80 ppm), and Ni (70 ppm) relative to Guibaré.

Petrography

Within quartz veins of the Guibaré prospect, tourmaline forms isolated crystals (400 μm), clusters or thin layers of small crystals (100 μm), or aggregates of very fine-grained crystals (<15 μm), grading to coarser grains in the border zones (Fig. 4B). In many cases, the crys-

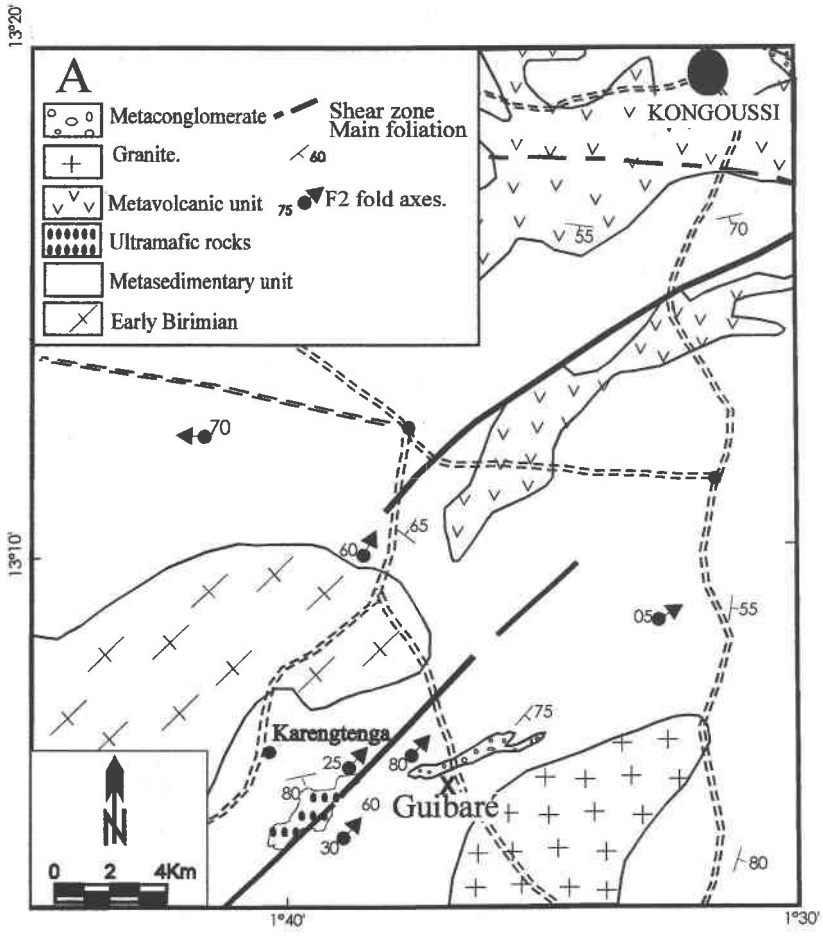

FIG. 2A. Geological map of the Guibaré prospect.

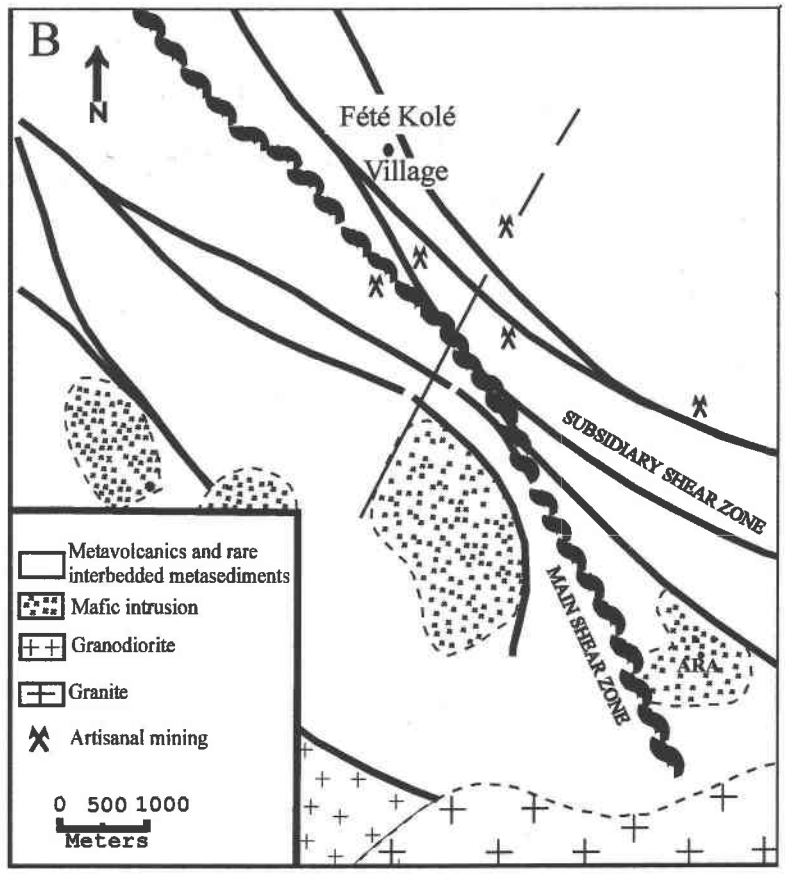

FIG. 2B. Geological map of the Fété Kolé prospect.

tals are optically zoned parallel to the c axis, with a light brown core and dark brown rim, some showing oscillatory zonation (Fig. 4C). These crystals have a distinctive brown pleochroism.

Tourmaline is locally abundant in the quartz veins of the Fété Kolé prospect, defining layers of tourmalinite of variable thickness (1 mm to 3 cm, Fig. 4D). These layers are cut by veinlets containing larger crystals of quartz (2 mm) and needles of tourmaline developed perpendicular to the border (Fig. 4E). Blue-green tourmaline also occurs in the sedimentary footwall, as large isolated prismatic crystals 3 mm in length. In both deposits, the dominant minerals are quartz and tourmaline, with the latter >5 to 10% by volume. Accessory sulfides (<0.1 vol.%) include pyrite, and more rarely, chalcopyrite and sphalerite. The gold is not associated with the rare sulfides, but rather is concentrated within layers of tourmaline as globular or «en plaquette» grains (< 2 mm), typically at the tips of the tourmaline crystals (Fig. 4F), and as small grains (< 100 μm) filling fractures in tourmaline. More rarely, gold occurs between grains of quartz, close to the tourmaline. In aggregates of tourmaline, no evidence of sulfides is visible, even at 500× magnification with the scanning electron microprobe (Fig. 5), indicating that small grains of gold (<10 μm) are directly attached to fine-grained tourmaline, along fractures and grain boundaries.

TOURMALINE

Chemical compositions

More than sixty electron-microprobe analyses of tourmaline were done using a CAMEBAX SX-50 instrument at the Laboratoire de Minéralogie, Toulouse (beam current of 10 nA, 15 kV, with counting times of 10 s at peak positions and 5 s for backgrounds). The following standards were used: wollastonite for Si and Ca, corundum for Al, $MnTiO_3$ for Mn and Ti, MgO for Mg, Fe_2O_3 for Fe, Cr_2O_3 for Cr, albite for Na, sanidine for K, and topaz for F. The data were corrected using PAP (SX–50) procedures. Tourmaline formulae were

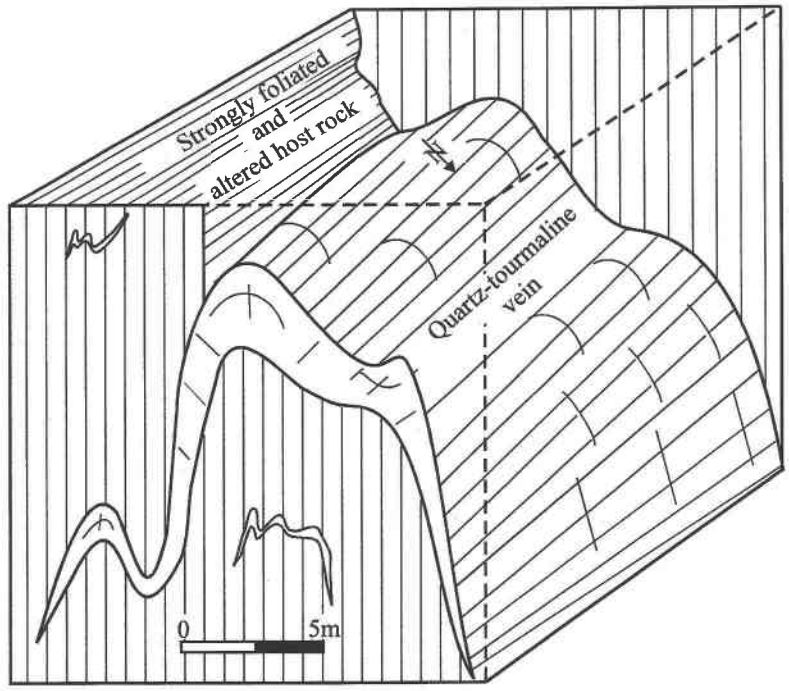

FIG. 3. Simplified geological section showing the geometry of tourmaline-quartz veins at Guibaré.

normalized to 31 (O, OH, F) atoms; representative compositions are given in Table 1. Atomic proportions in the structural formula vary within the following ranges: $^{X}(\square_{0.17-0.46}Na_{0.50-0.79}K_{0-0.02}Ca_{0-0.15})$ $^{Y}(Mg_{0.80-1.81}Fe_{0.62-1.60}Al_{0.17-0.62}Ti_{0-0.14}Cr_{0-0.03})$ $^{Z}Al_6$ $(BO_3)_3Si_{5.85-6.10}O_{18}$ $(OH, F)_1(OH)_3$. The fairly linear correlations shown in Figures 6A and B indicate that the dominant substitutions involved are the exchange vectors $FeMg_{-1}$ and $NaMg\square_{-1}Al_{-1}$ (Henry & Dutrow 1990, London & Manning 1995); this latter vector involves Mg*, Al* and Na*, which represent in essence the sum of the divalent, trivalent and monovalent cations (Mg* = Mg + Fe + Mn – Ti, Al* = Al + 2Ti, and Na* = Na + K). Tourmaline compositions for the two prospects show a limited uvite component, with Ca less than 0.2 atoms per formula unit. The incorporation of Ca appears to be controlled by variable substitutions such as $\square AlNa_{-1}Mg_{-1}$, $Ca_{0.5}\square_{0.5}Na_{-1}$, and $CaMgO\square_{-1}Al_{-1}(OH)_{-1}$ (Fig. 6C).

At Guibaré, the tourmaline corresponds compositionally to Mg-rich dravite, with Ca/(Ca + Na) < 0.06 and Fe/(Fe + Mg) values of 0.25 to 0.60 (Fig. 7). The dominant pattern of zoning reflects an increase in Fe/(Fe + Mg) from core to tip of the prisms. More rarely, tourmaline exhibits oscillatory zonation (Figs. 4C, 7) parallel to the *c* axis.

TABLE 1. REPRESENTATIVE COMPOSITIONS* OF TOURMALINE FROM GUIBARÉ AND FÉTÉ KOLÉ

	Gui T1c	Gui T1r	Gui T2μ	FK T1c	FK T1r	FK TQ1	FK fw1c	FK fw1i	FK fw1r
SiO_2 wt%	36.93	36.47	36.14	36.51	35.71	35.80	35.22	35.46	35.06
Al_2O_3	32.01	32.75	32.76	33.02	32.68	31.22	32.63	32.20	32.66
FeO	7.39	9.71	7.74	9.49	11.23	8.91	9.45	10.43	9.66
MnO	0.00	0.01	0.06	0.02	0.00	0.00	0.07	0.06	0.00
MgO	6.67	4.28	5.73	4.92	3.69	5.74	4.82	5.49	5.23
TiO_2	0.02	0.68	0.51	0.15	0.44	1.07	0.62	0.34	0.45
Cr_2O_3	0.00	0.06	0.04	0.04	0.00	0.09	0.00	0.00	0.03
CaO	0.09	0.13	0.12	0.21	0.16	0.28	0.21	0.52	0.82
Na_2O	2.06	1.82	2.03	1.55	1.93	2.05	1.93	2.15	2.06
K_2O	0.07	0.01	0.07	0.00	0.03	0.02	0.00	0.03	0.02
F	0.12	0.13	0.37	0.39	0.19	0.39	0.12	0.14	0.00
–O=F	–0.05	–0.05	–0.16	–0.16	–0.08	–0.16	–0.05	–0.06	0.00
Total	85.31	86.00	85.41	86.14	85.98	85.41	85.02	86.76	85.99
Si *apfu*	6.101	6.069	6.008	6.028	5.989	6.002	5.917	5.870	5.857
Al	6.232	6.423	6.418	6.425	6.459	6.168	6.460	6.281	6.430
Fe	1.020	1.351	1.076	1.310	1.575	1.249	1.327	1.443	1.349
Mn	0.000	0.001	0.008	0.003	0.000	0.000	0.010	0.008	0.000
Mg	1.643	1.062	1.420	1.211	0.923	1.435	1.207	1.355	1.303
Ti	0.002	0.085	0.064	0.019	0.055	0.135	0.078	0.042	0.057
Cr	0.000	0.008	0.005	0.005	0.000	0.012	0.000	0.000	0.004
Ca	0.016	0.023	0.021	0.037	0.029	0.050	0.038	0.092	0.147
Na	0.660	0.587	0.654	0.496	0.627	0.666	0.629	0.690	0.667
K	0.015	0.002	0.015	0.000	0.006	0.004	0.000	0.006	0.004

Points analyzed: micrograins (μ), core (c), interior (i) and rim (r) of prismatic crystals from tourmaline-rich veins (T), quartz-rich veins (TQ), and metasedimentary footwall (fw) of the Guibaré (Gui) and Fété Kolé (FK) deposits. * Electron-microprobe data.

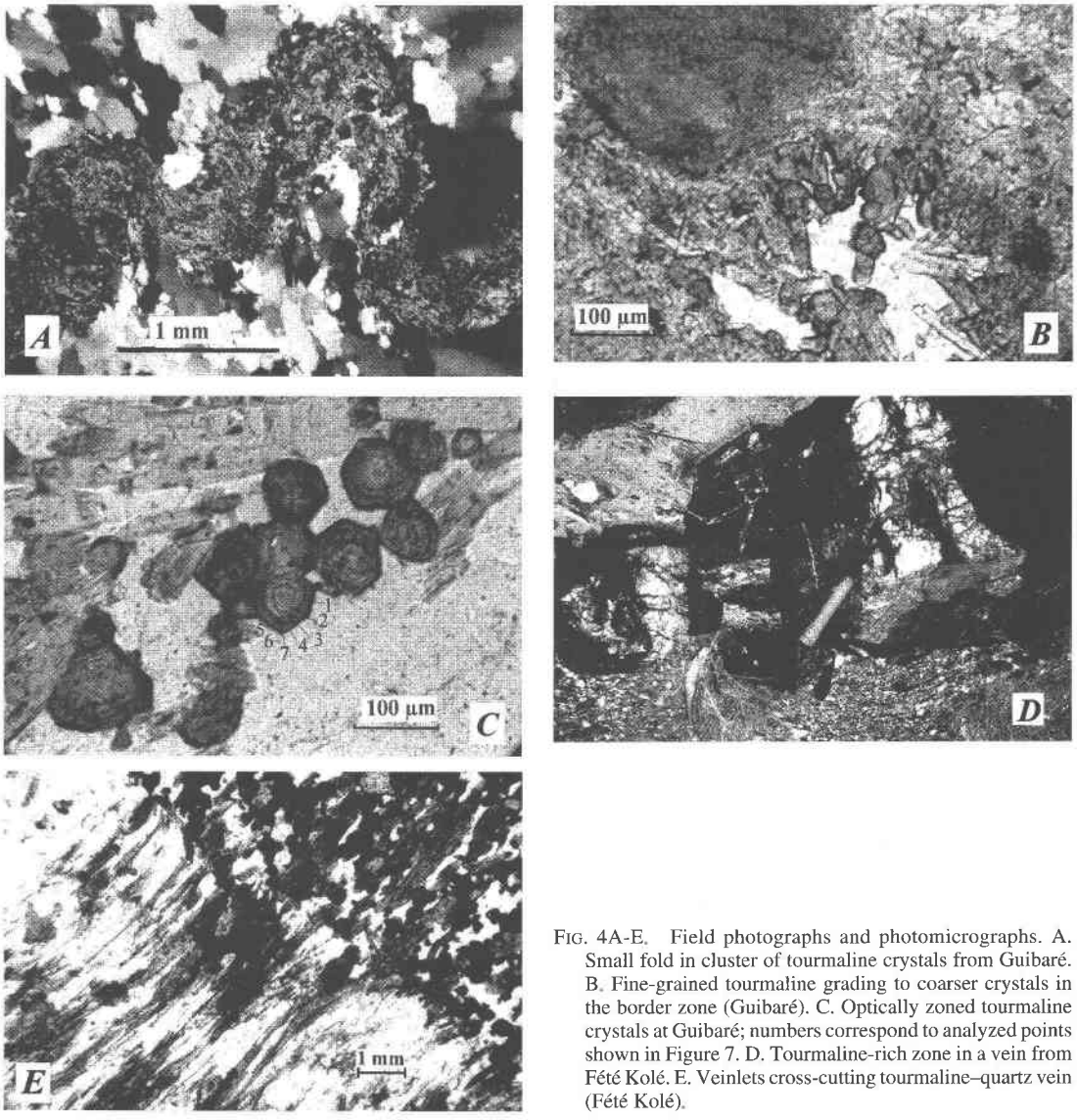

FIG. 4A-E. Field photographs and photomicrographs. A. Small fold in cluster of tourmaline crystals from Guibaré. B. Fine-grained tourmaline grading to coarser crystals in the border zone (Guibaré). C. Optically zoned tourmaline crystals at Guibaré; numbers correspond to analyzed points shown in Figure 7. D. Tourmaline-rich zone in a vein from Fété Kolé. E. Veinlets cross-cutting tourmaline–quartz vein (Fété Kolé).

At Fété Kolé, the compositions tend toward schorl, with Ca/(Ca + Na) values in the range 0.03 to 0.18 and Fe/(Fe + Mg) values in the range 0.40 to 0.70 (Fig. 7). These tourmaline grains exhibit a chemical zonation similar to those at Guibaré, except for the blue-green tourmaline hosted by the metasedimentary footwall, which displays an increase in Ca/(Ca + Na) from the core (0.05) to the rim (0.18).

Mössbauer and infrared data

A ^{57}Fe Mössbauer absorption spectrum over the range ±4 mm/s in 512 channels was recorded in the Laboratoire de Chimie de Coordination, Toulouse. The Mössbauer spectrometer is composed of a compact γ-ray detector system for high count-rates and a conventional constant-acceleration Mössbauer device (Wisel). A ^{57}Co (in Rh) source with nominal activity of 50 mCi was used. Spectra were obtained at room temperature and recorded on a Canberra multichannel analyzer. The isomer shift was recorded with respect to α-Fe metal. The sample thickness of the absorber was calculated for tourmaline samples according to the method of Rancourt *et al.* (1993); the value is approximately 100 mg of mineral per cm^2. Powders were finely ground under acetone (to minimize possible oxidation of iron) and placed in

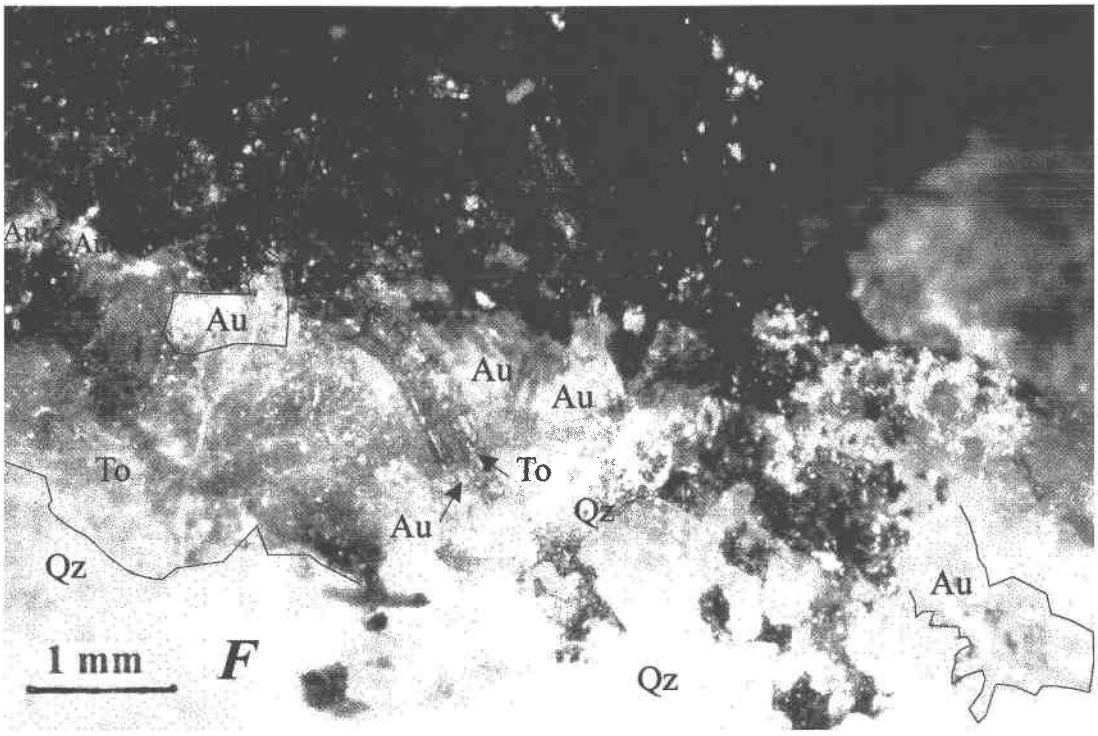

FIG. 4F. Gold at the tips of tourmaline crystals, Guibaré prospect.

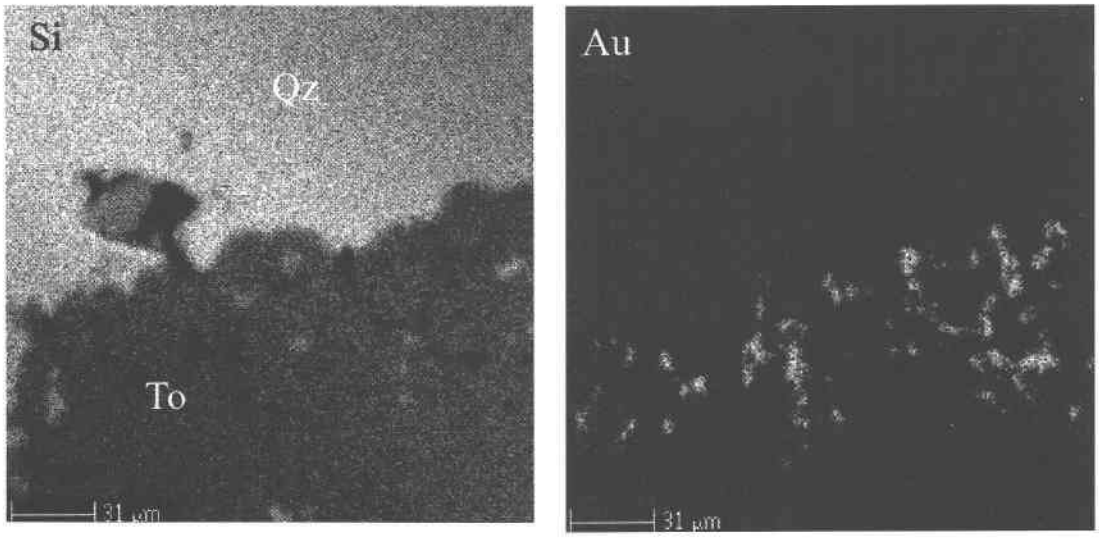

FIG. 5. Si$K\alpha$ and Au$K\alpha$ X-ray maps of small grains of gold filling fractures in tourmaline (Guibaré).

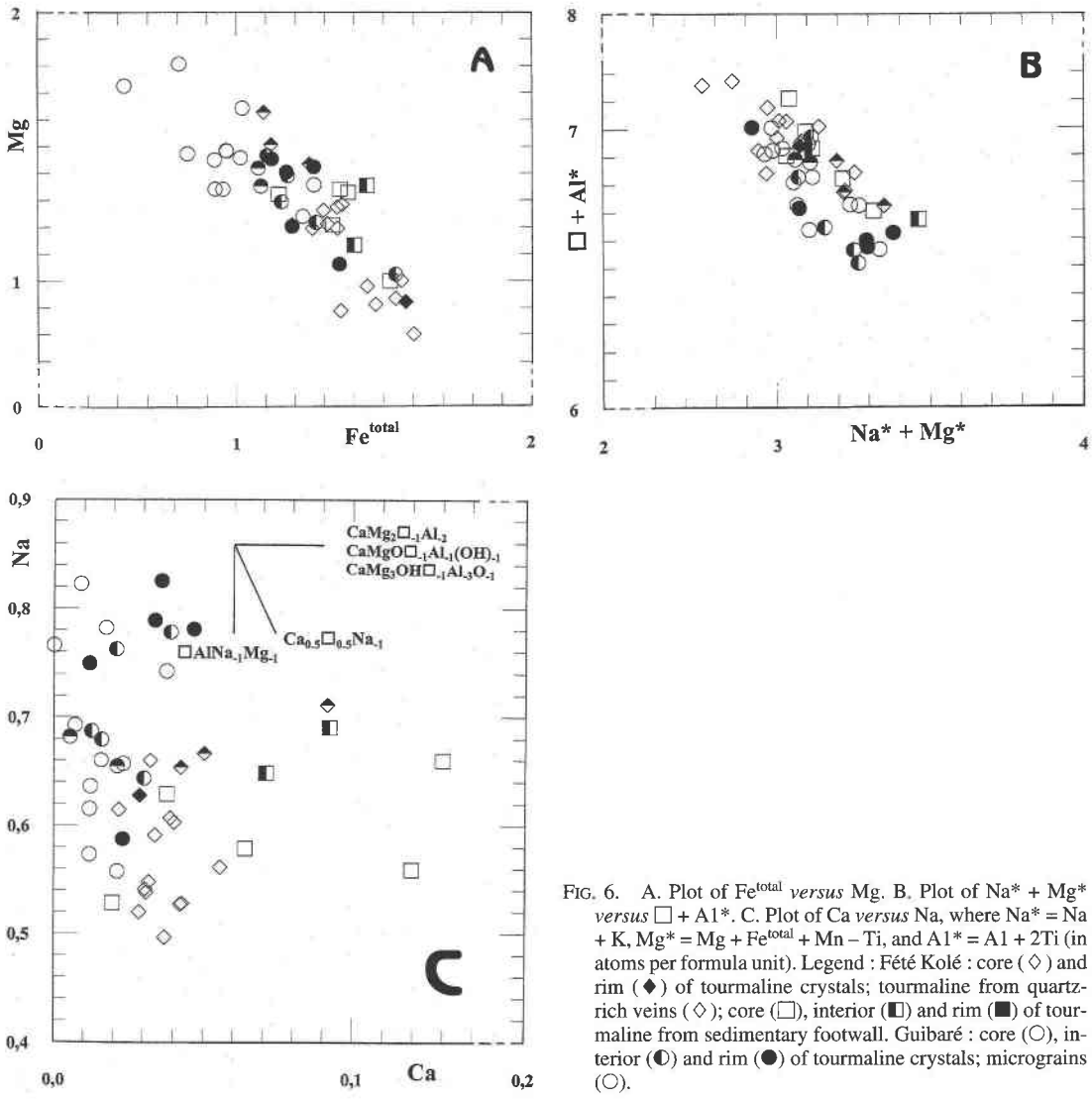

FIG. 6. A. Plot of Fe^{total} *versus* Mg. B. Plot of Na* + Mg* *versus* □ + A1*. C. Plot of Ca *versus* Na, where Na* = Na + K, Mg* = Mg + Fe^{total} + Mn – Ti, and A1* = A1 + 2Ti (in atoms per formula unit). Legend : Fété Kolé : core (◇) and rim (◆) of tourmaline crystals; tourmaline from quartz-rich veins (◇); core (□), interior (◧) and rim (■) of tourmaline from sedimentary footwall. Guibaré : core (○), interior (◐) and rim (●) of tourmaline crystals; micrograins (○).

the plexiglass sample holder. Lorentzian line shapes were assumed for deconvolutions, based on least-squares fitting procedures. The χ^2 and misfit values were used to measure the goodness of the computer fit.

Room-temperature Mössbauer spectra of the tourmaline samples (Figs. 8, 9) from Guibaré and Fété Kolé consist of three doublets (Table 2) with parameters characteristic of Fe^{3+} in the *Y*(9*b*) site, and Fe^{2+} in both *Y* and *Z*(18*c*) sites (Fuchs *et al.* 1995, 1998, Fig. 10). The attribution of the Fe^{2+} doublet having a quadrupole splitting around 1.60 mm/s is classically attributed to Fe^{2+} in the octahedrally coordinated *Z* site (Hermon *et al.* 1973, Gorelikhova *et al.* 1978, Kovorushkin *et al.* 1979, Saegusa *et al.* 1979, Fuchs *et al.* 1995). Recently, the possibility of the presence of Fe^{2+} at the *Z* site was rejected by Pieczka (1997), in light of significant variations in the crystal field. However, this octahedrally coordinated *Z* site, with an external location with respect to octahedra sharing a common edge, has dimensions smaller than the other octahedrally coordinated site, *Y*(9*b*). Logically, during establishment of the tourmaline structural formula, those *Y* sites contain cations with smaller ionic radii, such as Al and Fe^{3+} (Donnay & Buerger 1950, Buerger *et al.* 1962, Donnay & Barton 1972). However, structure refinements of tourmaline by Gorskaya *et al.* (1982), supplemented recently by Hawthorne *et al.* (1993) on dravite (with low Fe content), showed that Mg could occupy the *Z* site. In addi-

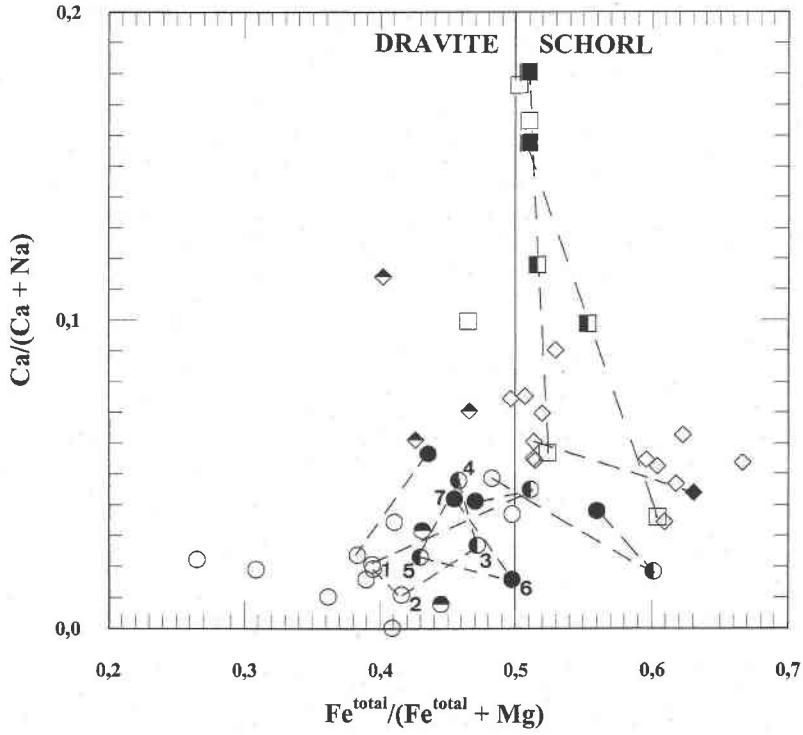

FIG. 7. Plot of tourmaline compositions. Numbers correspond to analyzed points across a color-zoned cross-section of a tourmaline prism, shown in Figure 4C. Symbols as in Figure 6.

tion, a tourmaline with approximately 6 atoms per formula unit (*apfu*) Al (6.05) was studied by Mössbauer spectroscopy (Hermon *et al.* 1973) and structurally by X-ray diffraction (Fortier & Donnay 1975). The combined results clearly indicate the presence of Fe^{2+} at the *Z* site. Results of Hawthorne *et al.* (1993) and Fortier & Donnay (1975) show clearly that the *Z* site also can accommodate, in addition to Al and Fe^{3+}, Mg and Fe^{2+}. These results are in agreement with crystallographic data: Mg in coordination number 6 has an ionic radius estimated at 0.72 Å *versus* 0.55 Å for Fe^{3+} and 0.61 Å for Fe^{2+}, whereas Al, the principal occupant of this site, has, under these conditions, an ionic radius of 0.535 Å. Site *Z* may accept cations having an ionic radius close to that of Fe^{2+}, insofar as the findings of Gorskaya *et al.* (1982) and Hawthorne *et al.* (1993) indicate clearly that Mg is present at the *Z* site. Consequently, Mg can be present at site *Z*, which does not exclude the presence there of Fe^{2+}.

TABLE 2. MÖSSBAUER PARAMETERS FOR TOURMALINE FROM GUIBARÉ AND FÉTÉ KOLÉ, AND CRYSTALLOGRAPHIC SITES OF Fe

Samples	δ	Δ	Oxidation state	Site	Goodness of fit (χ^2)	Ratio (%)
Guibaré	1.061(3)	2.380(2)	2+	*Y*(9*b*)		63
	1.063(3)	1.734(4)	2+	*Z*(18*c*)	0.739	32
	0.642(4)	0.735(4)	3+	*Y*(9*b*)		5
Fété Kolé	1.050(3)	2.332(8)	2+	*Y*(9*b*)		56
	1.007(6)	1.692(6)	2+	*Z*(18*c*)	0.901	22
	0.540(3)	0.673(4)	3+	*Y*(9*b*)		22

δ: isomer shift relative to Fe-metal, expressed in mm/s; Δ: quadrupole splitting, expressed in mm/s.

The major difference in the tourmaline between Guibaré and Fété Kolé lies in the Fe^{3+} content, 5% and 22%, respectively. Based on the Mössbauer results, mean structural formulae can be established in both deposits:

Guibaré: $^{X}(\square_{0.285}Na_{0.688}K_{0.007}Ca_{0.020})$
$^{Y}(Mg_{1.400}Fe^{2+}_{0.790}Al_{0.656}Ti_{0.056}Fe^{3+}_{0.050}Cr_{0.005})$
$^{Z}(Al_{5.750}Fe^{2+}_{0.250})\ (BO_3)_3Si_{6.034}O_{18}(OH, F)_1(OH)_3$

Fété Kolé: $^{X}(\square_{0.337}Na_{0.584}K_{0.004}Ca_{0.039})$
$^{Y}(Mg_{1.144}Fe^{2+}_{0.790}Al_{0.724}Fe^{3+}_{0.299}Ti_{0.042}Cr_{0.004})$
$^{Z}(Al_{5.728}Fe^{2+}_{0.272})\ (BO_3)_3Si_{5.994}O_{18}(OH, F)_1(OH)_3$

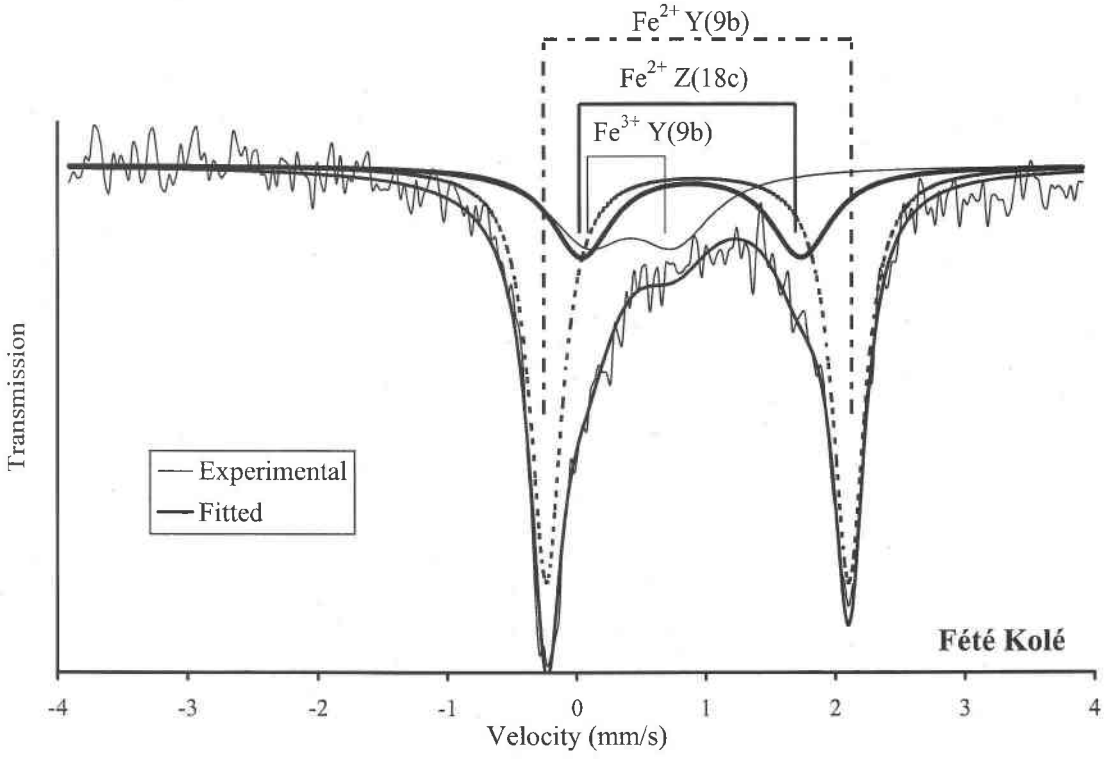

FIG. 8. Mössbauer spectra of Fété Kolé tourmaline at room temperature.

We performed FTIR (Fourier transform infrared) spectroscopy on powdered samples of tourmaline from Guibaré and Fété Kolé in order to verify the Mössbauer data and the possible structural or charge-balance-induced changes. The powder was included in KBr, and the mixture pressed as disks. The spectra were obtained with a Nicolet 560 spectrometer at scan 500 and resolution of 2 cm^{-1}.

Both spectra (Fig. 11) are roughly parallel in the 3800–3600 cm^{-1} domain. In FTIR spectra of tourmaline, absorption bands in the 3800–3600 cm^{-1} range are related to the inner hydroxyl group, whereas the 3600–3550 cm^{-1} band is normally assigned to the outer OH groups (Table 3). For tourmaline from Guibaré and Fété Kolé, the domain of the outer OH group is very different. In this domain, the outer OH groups are linked to one cation in the *Y* site and two cations in the *Z* site. The multiplicity of different occupancies of the *Y* and *Z* sites by Mg, Fe^{2+}, Fe^{3+}, and Al induces a broadening of the absorption bands. In the Guibaré sample, the 3486 cm^{-1} band is well marked and represents an OH group surrounded by 3 Al: 2Al in *Z* ↔ OH ↔ 1Al in *Y*. The 3732 cm^{-1} band is assigned to the 3 Mg^{2+}–OH stretching vibration; it corresponds to the 3738 cm^{-1} band observed in dravite by Gonzalez-Carreno *et al.* (1988). The 3724 cm^{-1} absorption band is assigned to a 2 $Mg^{2+}Fe^{2+}$–OH association, and the importance of both 3696 cm^{-1} ($Mg^{2+}2\,Fe^{2+}$–OH) and 3681 cm^{-1} ($3Fe^{2+}$–OH) bands are in good agreement with the results of the electron-microprobe analyses and the Mössbauer data. The 3632 and 3622 cm^{-1} absorption bands can be considered a

TABLE 3. ATTRIBUTION OF FTIR ABSORPTION BANDS, TOURMALINE FROM FÉTÉ KOLÉ AND GUIBARÉ

Fété Kolé	Guibaré		Attribution
	3486	3 OH	3Al
3551	3547	"external" group	
3566	3566	linked to 1 *Y*(9*b*) and 2 *Z*(18*c*) sites	2Al 1R^{2+}
3629	3629	1 OH	$2Fe^{2+}$Mg–OH >>> □
3649	3647	"internal" group	$3Fe^{2+}$–OH >>> □
3670	3670	linked to	3Fe–OH >>> Na
3689	3688	3 *Y*(9*b*) sites	3Fe–OH >>> Ca
	3701	and pointing	
3711	3712	toward (>>>)	2Mg1Fe–OH >>> Na
3725	3726	1 *X*(3*a*) site	2Mg1Fe–OH >>> Ca
3731	3732		3Mg–OH >>> Na
	3744		3Mg–OH >>> Ca

Absorption bands in wavenumbers (cm^{-1}).

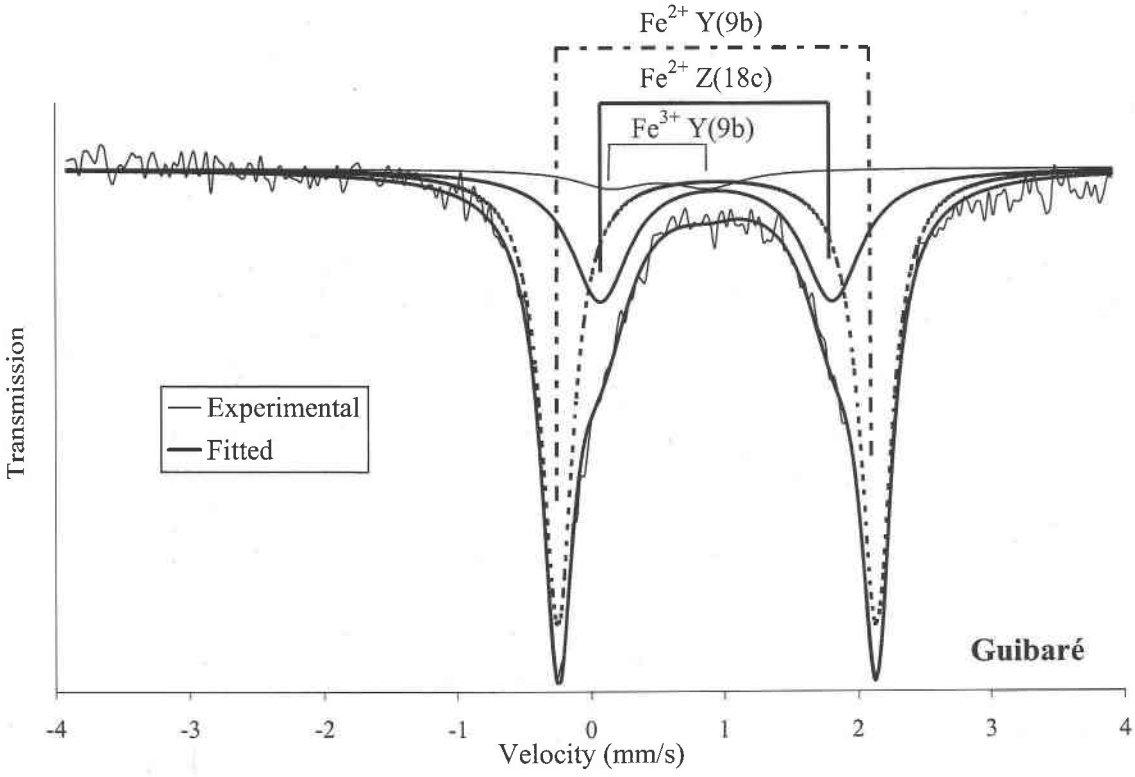

FIG. 9. Mössbauer spectra of Guibaré tourmaline at room temperature.

replica of the previous doublets, and are assigned to inner hydroxyl groups bonded to (or adjacent to) three divalent cations in the *Y* (9*b*) site, pointing toward a vacant (□) *X* (3*a*) site. The relative intensity of this band, compared to that of the 3622 – 3632 cm^{-1} doublet, may be related to the increase of the molar absorbtivity of the OH group pointing toward a vacant site instead of an occupied one. This difference was emphasized for other minerals by Skogby & Rossman (1989); it is due not only to the additivity of the $3M^{2+}$–OH → (□) and ($2M^{2+}$, $1M^{3+}$)–OH → Na absorption bands, but also to the change in ratio between inner and outer OH groups. The bands observed near 3560–3550 cm^{-1} are assigned to the outer OH groups, which are bonded to one cation in the *Y* site and two cations in the *Z* site. The high number of combinations explains the width of the absorption band. In tourmaline having an important contribution of Al in the *Y* site, a band is normally present at 3485 cm^{-1} and is assigned to an $^{Y}(Al^{3+})\ ^{Z}(2Al^{3+})$ – OH association. This band is weak at Guibaré and totally absent at Fété Kolé, in agreement with the electron-microprobe data. The 3533 cm^{-1} band can obviously be assigned to $^{Y}(Fe^{3+})\ ^{Z}(2Al^{3+})$–OH or $^{Y}(Fe^{3+})\ ^{Z}(Al^{3+} + Fe^{2+})$–OH, and the 3560 cm^{-1} band, to a normal $R^{2+}(Fe^{2+}$ or $Mg^{2+})$–OH–$2Al^{3+}$ association, whereas the band at 3544 cm^{-1} possibly corresponds to a R^{2+}–OH–$Fe^{2+}Al^{3+}$ linkage.

Calculation of charge balance in tourmaline from both Guibare and Fété Kolé shows a charge excess that can be compensated by the dehydroxylation of one OH. The difference between the two samples of tourmaline is not significant regarding the relative errors in electron-microprobe and Mössbauer data, but the difference in their absorbance, attributed to the outer and inner OH groups in Guibaré and Fété Kolé, can be attributed to a stronger dehydroxylation of the outer groups at Fété Kolé. Experimental work on natural and synthetic tourmalines has shown that experimental oxidation of Fe^{2+} to Fe^{3+} is charge-compensated by dehydroxylation of the outer OH group (Fuchs & Lagache 1994). At Guibaré, the tourmaline shows a stronger absorption in this domain than in the 3800–3600 cm^{-1} one, in full agreement with the attribution to the three outer OH groups that bond one cation in *Y* with two cations in *Z*, whereas the 3800–3600 cm^{-1} area is related only to the inner OH group. In the Fété Kolé sample, the difference in absorbance is weak and can be attributed to an extensive deprotonation of the external OH groups. Such deprotonation seems to be related to oxidation of Fe^{2+} to Fe^{3+}, according to the exchange vector $Fe^{3+}O$

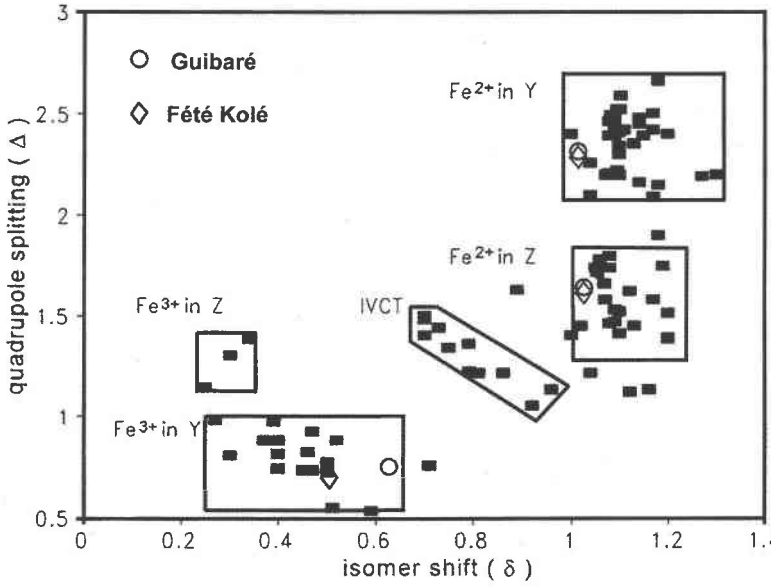

FIG. 10. Values of isomer shift (δ) and quadrupole splitting (Δ) for tourmaline from Guibaré and Fété Kolé. Values from other samples of natural tourmaline [■ : Fuchs *et al.* (1998), and references therein].

$(Fe^{2+}OH)_{-1}$. This can be clearly observed on a plot of $(R^{+} + R^{2+})$ in *X* and *Y* sites *versus* R^{3+} in *Y* and *Z* sites, the compositions of tourmaline plotting along and between the dehydroxylation and alkali-deficiency lines from a schorl or dravite component (Fig. 12).

COMPOSITIONS OF GOLD

The gold contains between 10 and 28% Ag, which is the same fineness as the gold associated with sulfides in other deposits of the Birimian greenstone belts of Burkina Faso, for example in mesothermal Au–quartz veins without tourmaline, *e.g.,* Taparko and Gangaol (Bourges *et al.* 1994) and Poura (Sanogo & Prost 1993), and in a disseminated Au deposit hosted by albitite, at Larafella (Bamba *et al.* 1997) and by albitite and listvenite, at Loraboué (Béziat *et al.* 1998). These compositions differ from that in the Loulo deposit, where very pure gold (1% Ag only) is developed in fissures and at the surface of pyrite grains (Milési *et al.* 1992).

DISCUSSION

In comparison with available compositions of tourmaline associated with Au deposits taken from the literature (*e.g.,* Slack 1996), our tourmaline data clearly differ from those for tourmaline in Bulagidun, Sulawesi (Lubis *et al.* 1994), Bin Yauri area, Nigeria (Garba 1996), Passagem de Mariana, Brasil, and Ming, Canada (quoted in Slack 1996) by its higher Al contents, and from that in Buffalo-Ankerite, Canada (King & Kerrich 1989), and Golden Dyke dome, Australia (Plimer 1986) by its higher Fe contents (Fig. 13). On the other hand, the tourmaline data from Guibaré and Fété Kolé mostly overlap those from the Timmins–Porcupine district of Ontario (King & Kerrich 1989), the inner alteration zone of the Jack Creek deposit, Montana, and the outer zone of the Lincoln Hill deposit, Nevada (Fuchs & Maury 1995). In comparison with the well-known Loulo Au deposit in Mali, our data differ slightly from those for tourmaline filling veins in stockworks, and markedly from those for tourmaline replacing a sandstone matrix (Dommanget *et al.* 1985, Milési *et al.* 1992).

In the Guibaré and Fété Kolé deposits, the tourmaline–quartz veins are strongly folded in regional shear-zones. Compositions of tourmaline differ at the two prospects: at Guibaré, the tourmaline is dravite, and the host rocks are ultrabasic to basic, with a high Mg/(Mg + Fe) value (0.75), whereas at Fété Kolé, the tourmaline is schorl, and the host rocks are metasedimentary and metavolcanic, with a low Mg/(Mg + Fe) value (0.35). This difference in tourmaline composition can be related to the compositional difference of their respective host-rocks rather than the chemistry of the hydrothermal fluid, suggesting low water:rock conditions of the hydrothermal system (Slack 1996, Jiang *et al.* 1998). Occurrence of the discontinuous and oscillatory compositional zonations suggest complex chemical varia-

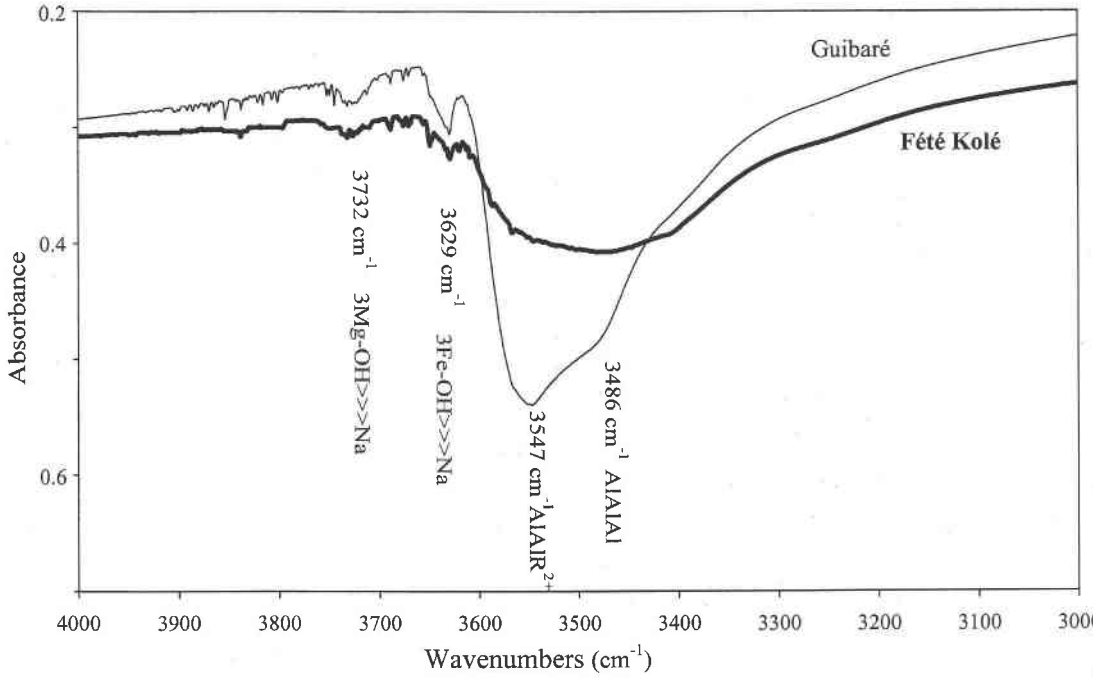

FIG. 11. FTIR spectra of tourmaline in the 4000–3000 cm^{-1} domain.

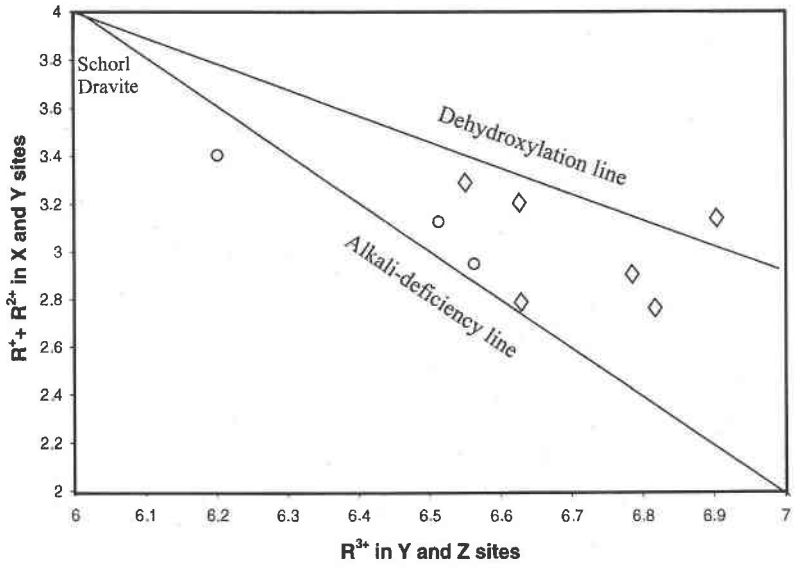

FIG. 12. ($R^+ + R^{2+}$) in *X* and *Y* sites *versus* R^{3+} in *Y* and *Z* sites. Symbols as in Figure 10.

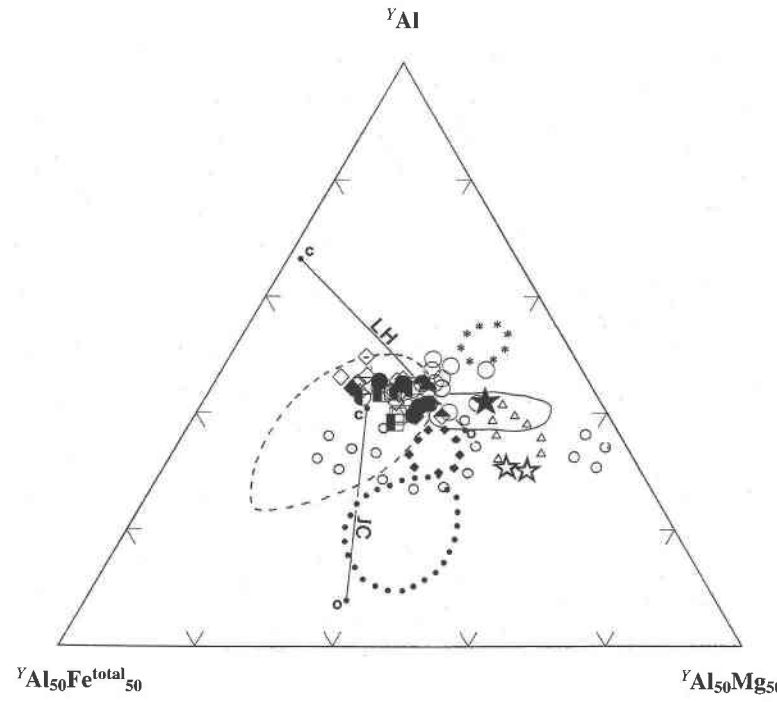

FIG. 13. Compositional fields of tourmaline. ---: Timmins-Porcupine Au deposits, Ontario (King & Kerrich 1989), ___: Golden Dyke dome Au deposit, Australia (Plimer 1986), ***: Buffalo-Ankerite Au deposit, Ontario (King & Kerrich 1989), ○○○: Passagem de Mariana Au deposit, Brasil (in Slack 1996), ◆◆◆: Bin Yauri Au deposit, Nigeria (Garba 1996), ●●●: Bulagidun Cu–Au deposit, Sulawesi (Lubis *et al.* 1994), ΔΔΔ: Ming Cu–Au deposit, Ontario (in Slack 1996). Tie-lines: central (c) and outer (o) zones of hydrothermal fields from Lincoln Hill (LH) Ag–Au deposit, Nevada, and Jack Creek (JC) Ag–Au deposit, Montana (mean values; Fuchs & Maury 1995). Loulo Au deposit, Mali: tourmaline replacing the sandstone matrix (☆) or filling veins (★, unpublished data from A. Dommanget). Symbols for Guibaré and Fété Kolé as in Figure 6.

tions of fluids during crystal growth, in particular in Fe/(Fe+Mg) value. Like the feruvite from the Sullivan Pb–Zn–Ag deposit (Jiang *et al.* 1996), enrichment of Ca in the blue-green rims of the tourmaline from the metasedimentary host-rock at Fété Kolé could result from the local breakdown of Ca-rich minerals. Therefore, as in most tourmalines from quartz veins associated with polymetallic sulfides (Slack *et al.* 1993, Slack 1996), we consider the primary growth of tourmaline to record the presence of a B-rich fluid that was chemically buffered by the host rocks.

The most common type of gold occurrence is in quartz-lode deposits, in which native gold is either attached to sulfides (particularly pyrite and arsenopyrite) or localized in the quartz gangue next to sulfides. In the same way, in gold deposits hosted by tourmalinized rocks (*e.g.,* Loulo, Golden Dyke dome, Timmins–Porcupine district), gold is associated with the sulfide mineralization. A major exception, however, occurs at the Sigma mine, Abitibi, Quebec (Robert & Brown 1986, Robert & Kelly 1987), in which most grains are attached to tourmaline along fractures and grains boundaries. Recently, in a morphological study of ore at the Sigma mine, Michel & Giuliani (1996) reported that the particles of gold have shapes typical of tourmaline casts.

At Guibaré and Fété Kolé, the economic and visible gold is essentially and closely linked to the formation of tourmaline, reflecting two main stages of mineral deposition, related to early growth and later deformation: a vein-filling event, with deposition of quartz and tourmaline in extensional veins, and a post-filling event, with deposition of gold grains at the tips of crystals and in fractures in tourmaline.

Mössbauer and infrared spectroscopic data indicate the presence of ferric iron in the tourmaline, a feature correlated with a deprotonation reaction. The crystallochemical distribution of iron (Fe^{2+} in the *Z* site and Fe^{2+} and Fe^{3+} in the *Y* site) can only be explained by the ini-

tial formation of tourmaline in a reducing environment, and subsequent overprinting by more oxidizing fluids (Maury & Fuchs 1991), the *Y* site being the only one sensitive to late oxidation (Fuchs *et al.* 1995). Such Fe^{3+}-rich tourmaline has been interpreted to indicate relatively oxidizing environments for mineralization in a variety of types of deposit (London & Manning 1995, Slack 1996, Lynch & Ortega 1997). This hypothesis is corroborated by the rarity of sulfides in the two prospects. The difference in Fe^{3+} contents of the tourmaline from Guibaré and Fété Kolé could be related to the nature of the tourmaline itself (dravite in Guibaré, schorl in Fété Kolé), the oxidizing nature of the fluid, the location in the hydrothermal system (central or distal part), the extent of tectonic deformation, and possibly other factors.

To assess the causes of gold deposition, we require information about the composition of the hydrothermal fluid and the mode of transport of the gold. It is known that the solubility of Au in hydrothermal fluids may be controlled by thiosulfate complexing as $Au(HS)_2^-$. The destabilization of such complexes and deposition of gold can be achieved by an increase or decrease in pH of the fluid (Fyfe & Kerrich 1984, Seward 1989) or by a sudden drop in fluid pressure (Boullier & Robert 1992). Both conditions are met at the Guibaré and Fété Kolé deposits. The habit of gold grains indicates that deposition of the gold occurred as fluid entered in cavities and fractures in the tourmaline. Moreover, the deprotonation accompanying oxidation of the tourmaline could induce the chemical changes that caused gold deposition, according to the reaction proposed by several authors (*e.g.*, Huston *et al.* 1992): $4\ Au(HS)^-_2 + 2\ H_2O + 4\ H^+ = 4\ Au + 8\ H_2S_{(aq)} + O_2$. Gold reduction on earlier-formed tourmaline has previously been documented at the Sigma mine; Michel & Giuliani (1996) proposed that tourmaline, like sulfide minerals, may allow the reduction of gold on their surfaces because of the differences in normal oxidation potentials between Fe^{2+}/Fe^{3+} and Au^0/Au^+.

Throughout the Birimian greenstone belts of Burkina Faso, discordant mesothermal mineralization (auriferous arsenopyrite + sulfides and Au-bearing quartz veins) has generally been considered as representing the economically most important type of deposit (Huot *et al.* 1987, Milési *et al.* 1989, 1992, Sanogo & Prost 1993, Bourges *et al.* 1994). However, recent studies (Bamba *et al.* 1997, Béziat *et al.* 1998) have identified a new type of deposit, consisting of disseminated gold associated with albitite and listvenite. Thus, the Au-bearing tourmaline–quartz veins that we document here could represent another attractive target for Au prospection in Burkina Faso.

Acknowledgements

We are grateful to J.F. Slack, D.J. Henry and an anonymous reviewer for helpful comments and suggestions that improved this paper. We also thank R.F. Martin for constructive reviews. This study was carried out with the financial support of the Burkina Faso – France Cooperation Project (Campus research contract "Cartographie géologique appliquée à la recherche minière au Burkina Faso"). The authors gratefully acknowledge B.H.P. for access to exploration properties, and A. Dommanget for supplying samples and unpublished data from Loulo. We thank Dr. Philippe de Parseval for helpful assistance in electron-microprobe analyses at the Université Paul Sabatier.

References

Bamba, O., Béziat, D., Bourges, F., Debat, P., Lompo, M., Parizot, J.C. & Tollon, F. (1997): Nouveau type de gisement aurifère dans les ceintures de roches vertes birimiennes du Burkina Faso: les albitites de Larafella. *J. Afr. Earth Sci.* **25**, 369-381.

Béziat, D., Bourges, F., Debat, P., Lompo, M., Tollon, F. & Zonou, S. (1998): Albitite et listvénite: sites de concentration aurifère inédits dans les ceintures de roches vertes birimiennes du Burkina Faso. *Bull. Soc. Géol. Fr.* **169**, 563-571.

Boullier, A.-M. & Robert, F. (1992): Palaeoseismic events recorded in Archaean gold–quartz vein networks, Val d'Or, Abitibi, Québec, Canada. *J. Struct. Geol.* **14**, 161-179.

Bourges, F., Debat, P., Grandin, G., Parizot, J.C., Tollon, F., Baras, E. & Ouedraogo, M.F. (1994): Relations entre cristallisations de quartz et concentrations aurifères (exemple des filons aurifères du Birimien du Burkina Faso, Afrique de l'Ouest). *C.R. Acad. Sci. Paris* **319**, *sér.* **II**, 543- 550.

Buerger, M.J., Burnham, C.W. & Peacor, D.R. (1962): Assessment of the several structures proposed for tourmaline. *Acta Crystallogr.* **15**, 583-590.

Dommanget, A., Diallo, A. & Guilloux, L. (1985): Un nouveau type de gisement d'or, Loulo (Mali). *Chron. Rech. Minières Fr.* **53**(481), 5-18.

Donnay, G. & Barton, R., Jr. (1972): Refinement of the crystal structure of elbaite and the mechanism of tourmaline solid solution. *Tschermaks Mineral. Petrogr. Mitt.* **18**, 273-286.

_____ & Buerger, M.J. (1950): The determination of the crystal structure of tourmaline. *Acta Crystallogr.* **3**, 379-388.

Fortier, S. & Donnay, G. (1975): Schorl refinement showing composition dependence of the tourmaline structure. *Can. Mineral.* **13**, 173-177.

Fuchs, Y. & Lagache, M. (1994): Changes in iron oxidation state and deprotonation induced by annealing of natural tourmalines. *Int. Mineral. Assoc., 16th General Meeting (Pisa)*, 129 (abstr.).

_____, _____ & Linares, J. (1998): Fe-tourmaline synthesis under different T and fO_2 conditions. *Am. Mineral.* **83**, 525-534.

_____, _____, _____, MAURY, R. & VARRET, F. (1995): Mössbauer and optical spectrometry of selected schorl–dravite tourmalines. *Hyperfine Interaction* **96**, 245-248.

_____ & MAURY, R. (1995): Borosilicate alteration associated with U–Mo–Zn and Ag–Au–Zn deposits in volcanic rocks. *Mineral. Deposita* **30**, 449-459.

FYFE, W.S. & KERRICH, R. (1984): Gold: natural concentration processes. *In* Gold'82: the Geology, Geochemistry and Genesis of Gold Deposits (R.P. Foster, ed.). A.A. Balkema, Rotterdam, The Netherlands (99-127).

GARBA, I. (1996): Tourmalinization related to Late Proterozoic – Early Palaeozoic lode gold mineralization in the Bin Yauri area, Nigeria. *Mineral. Deposita* **31**, 201-209.

GONZALEZ-CARRENO, T., FERNANDEZ, M. & SANZ, J. (1988): Infrared and electron microprobe analysis of tourmalines. *Phys. Chem. Minerals* **15**, 452-460.

GORELIKHOVA, N.V., PERFIL'YEV, YU D. & BUBESHKIN, A.M. (1978): Mössbauer data on distribution of Fe ions in tourmaline. *Int. Geol. Rev.* **20**, 982-990.

GORSKAYA, M.G., FRANK-KAMENETSKAYA, O.V., ROZHDESTVENSKAYA, I.V. & FRANK- KAMENETSKII, V.A. (1982): Refinement of the crystal structure of Al-rich elbaite, and some aspects of the crystal chemistry of tourmalines. *Sov. Phys. Crystallogr.* **27**, 63-66.

GUSTAFSON, L.B. (1995): Magmatism, metamorphism, and deformation at Hemlo, Ontario, and the timing of Au–Mo mineralization in the Golden Giant mine – a discussion. *Econ. Geol.* **90**, 1341-1342.

HAWTHORNE, F.C., MACDONALD, D.J. & BURNS, P.C. (1993): Reassignment of cation site occupancies in tourmaline: Al–Mg disorder in the crystal structure of dravite. *Am. Mineral.* **78**, 265- 270.

HENRY, D.J. & DUTROW, B.L. (1990): Ca substitution in Li-poor aluminous tourmaline. *Can. Mineral.* **28**, 111-124.

HERMON, E., SIMKIN, D.J., DONNAY, G. & MUIR, W.B. (1973): The distribution of Fe^{2+} and Fe^{3+} in iron bearing tourmalines: a Mössbauer study. *Tschermaks Mineral. Petrogr. Mitt.* **19**, 124-132.

HUOT, D., SATTRAN, V. & ZIDA, P. (1987): Gold in Birimian greenstone belts of Burkina Faso, West Africa. *Econ. Geol.* **82**, 2033-2044.

HUSTON, D.L., BOTTRILL, R.S., CREELMAN, R.A., LIN, KHIN ZAW, RAMSDEN, T.R., RAND, S.W., GEMMELL, J.B., JABLONSKI, W., SIE, S.H. & LARGE, R.R. (1992): Geologic and geochemical controls on the mineralogy and grain size of gold-bearing phases, eastern Australian volcanic-hosted massive sulfide deposits. *Econ. Geol.* **87**, 542-563.

JIANG, SHAO-YONG, PALMER, M.R., MCDONALD, A.M., SLACK, J.F. & LEITCH, C.H.B. (1996): Feruvite from the Sullivan Pb–Zn–Ag deposit, British Columbia. *Can. Mineral.* **34**, 733-740.

_____, _____, SLACK, J.F. & SHAW, D.R. (1998): Paragenesis and chemistry of multistage tourmaline formation in the Sullivan Pb–Zn–Ag deposit, British Columbia. *Econ. Geol.* **93**, 47-67.

KING, R.W. & KERRICH, R. (1989): Chromian dravite associated with ultramafic-rock-hosted Archean lode gold deposits, Timmins–Porcupine district, Ontario. *Can. Mineral.* **27**, 419-426.

KOVORUSHKIN, V.V., KUZMIN, V.I. & BELOV, V.F. (1979): Mössbauer studies of structural features of tourmaline of various genesis. *Phys. Chem. Minerals* **4**, 209-220.

LONDON, D. & MANNING, D.A.C. (1995): Chemical variation and significance of tourmaline from southwest England. *Econ. Geol.* **90**, 495-519.

LUBIS, H., PRIHATMOKO, S. & JAMES, L.P. (1994): Bulagidun prospect: a copper, gold and tourmaline bearing porphyry and breccia system in northern Sulawesi, Indonesia. *J. Geochem. Expl.* **50**, 257-278.

LYNCH, G. & ORTEGA, J. (1997): Hydrothermal alteration and tourmaline–albite equilibria at the Coxheath porphyry Cu–Mo–Au deposit, Nova Scotia. *Can. Mineral.* **35**, 79-94.

MAURY, R. & FUCHS, Y. (1991) : Tourmalines structural refinement based on Mössbauer spectrometry. *EUG VI (Strasbourg), Terra Cognita* **3**, 8 (abstr.).

MICHEL, D. & GIULIANI, G. (1996) : Habit and composition of gold grains in quartz veins from greenstone belts : implications for mechanisms of precipitation of gold. *Can. Mineral.* **34**, 513-528.

MILÉSI, J.P., FEYBESSE, J.L., LEDRU, P., DOMMANGET, A., OUEDRAOGO, M.F., MARCOUX, E., PROST, A., VINCHON, C., SYLVAIN, J.P., JOHAN, V., TEGYEY, M., CALVEZ, J.Y. & LAGNY, P. (1989) : Gold mineralization in West Africa; its relation to lower Proterozoic lithostructural evolution. *Chron. Rech. Minières Fr.* **497**, 3-98.

_____, LEDRU, P., FEYBESSE, J.L., DOMMANGET, A. & MARCOUX, E. (1992) : Early Proterozoic ore deposits and tectonics of the Birimian orogenic belt, West Africa. *Precambrian Res.* **58**, 305-344.

PIECZKA, A. (1997) : Statistical interpretation of structural parameters of tourmalines : iron ordering in octahedral sites. *In* Tourmaline 1997 (Nové Mesto na Morave, Czech Republic), 70-71 (abstr.).

_____ & KRACZKA, J. (1997) : Thermal oxidation of Fe^{2+} ions in the schorl-dravite series and its significance in the analysis of distribution of Fe^{2+} octahedral ions. *In* Tourmaline 1997 (Nové Mesto na Morave, Czech Republic), 72-73 (abstr.).

PLIMER, I.R. (1986) : Tourmalinites from the Golden Dyke dome, northern Australia. *Mineral. Deposita* **21**, 263-270.

RANCOURT, D.G., MCDONALD, A.M., LALONDE, A.E. & PING, J.-Y. (1993) : Mössbauer absorber thicknesses for accurate site populations in Fe-bearing minerals. *Am. Mineral.* **78**, 1-7.

ROBERT, F. & BROWN, A.C. (1986) : Archean gold-bearing quartz veins at the Sigma mine, Abitibi greenstone belt, Quebec. II. Vein paragenesis and hydrothermal alteration. *Econ. Geol.* **81**, 593-616.

_____ & KELLY, W.C. (1987) : Ore-forming fluids in Archean gold-bearing quartz veins at the Sigma mine, Abitibi greenstone belt, Quebec, Canada. *Econ. Geol.* **82**, 1464-1482.

SAEGUSA, N., PRICE, D.C. & SMITH G. (1979) : Analysis of the Mössbauer spectra of several iron-rich tourmalines (schorls). *J. Phys. (Paris)* **40**, 456-459.

SANOGO, A.D. & PROST, A.E. (1993) : Evolution synchrone des déformations et des minéralisations dans le filon aurifère de Poura (province du Mohoun, Burkina Faso). *Pangea* **20**, 23-29.

SEWARD, T.M. (1989) : The hydrothermal chemistry of gold and its implications for ore formation : boiling and conductive cooling as examples. *Econ. Geol., Monogr.* **6**, 398-404.

SKOGBY, H. & ROSSMAN, G.R. (1989) : OH^- in pyroxene : an experimental study of incorporation mechanisms and stability. *Am. Mineral.* **74**, 1059-1069.

SLACK, J.F. (1996) : Tourmaline associations with hydrothermal ore deposits. *In* Boron : Mineralogy, Petrology, and Geochemistry (E.S. Grew & A.M. Anovitz, eds.). *Rev. Mineral.* **33**, 559-643.

_____, PALMER, M.R., STEVENS, B.P.J. & BARNES, R.G. (1993) : Origin and significance of tourmaline-rich rocks in the Broken Hill district, Australia. *Econ. Geol.* **88**, 505-541.

Received July 13, 1998, revised manuscript accepted March 17, 1999.